Describing intermittent processes in the ocean: Univariate and bivariate multiscaling procedures

Laurent Seuront

Ecosystem Complexity Research Group, CNRS UPRESA 8013 ELICO, BP 80, F-62930, Wimereux, France

François Schmitt

Department of Fluid Mechanics, Vrije Universiteit Brussel, Pleinlaan 2, B-1050 Brussels, Belgium

Abstract. Univariate and bivariate procedures for investigating the properties of single and joint intermittent stochastic processes are presented. They allow the characterization of all the statistics of intermittent variables using a set of three basic parameters in the multifractal framework, whatever the scales and the intensity. The multifractal formalism is then extended to more than one variable to investigate the degree of dependence among random fields by examining the nature of their joint distribution. These formalisms, which do not require any assumption about the spectrum or the probability distribution of the data sets under consideration, are finally illustrated, first, by studying the properties of turbulent velocity fluctuations recorded in a laboratory grid-generated turbulence experiment and in the ocean using a high-frequency free-fall profiler. Second, we investigate the distributions of temperature, salinity and *in vivo* fluorescence (a proxy of phytoplankton biomass) time series recorded in the coastal waters of the Southern Bight of the North Sea, as well as their potential correlation.

Introduction

Considering the current awareness of the intermittent nature of both physical and biological patterns and processes in marine sciences (*Gibson*, 1991; *Pascual et al.*, 1995; *Seuront et al.*, 1996a, 1999; *Jou*, 1997; *Jiménez*, 2000), and the emergence of hot topics such as those related to thin-layer properties (*Cowles et al.*, 1998; *Osborn*, 1998), there is a real need to focus on the precise nature of both single intermittent variables and the degree of correlations between joint intermittent variables, especially those related to physics and biology.

Recent theoretical and empirical developments, conducted both on turbulent energy dissipation rates and on the associated passive scalars distributions, have demonstrated the multiscale properties of intermittent processes (*Pascual et al.*, 1995; *Seuront et al.*, 1996a, b, 1999, 2001a, b; *Lovejoy et al.*, 2001). The large numbers of modeling approaches devoted to the structure of turbulent flows have only provided description at a very limited range of scales. Indeed, neither Gaussian diffusion models (*Visser*, 1997) nor direct numerical simulations (*Yamazaki et al.*, 1991) possess a way to change the scale upward or downward. In contrast, scale change is natural for multifractal processes (*Seuront et al.*, 1999). Moreover, Gaussian processes are determined by only two moments, while the first three moments of empirical processes are usually provided to characterize them. In the statistical framework of multifractals, we propose a more global approach since we provide all the moments (even non-integers), giving as much statistical information as the study of probability density directly.

The procedures used to test for independence between two processes, based on second order statistics analysis (i.e., correlation), become fallacious for intermittent non-Gaussian fields. It is then necessary to test for independence by studying joint moments of all orders. In addition, more recent procedures based on examination of probability density functions do not deal with the multiscaling properties of intermittent fields.

In this paper, first we define the concept of intermittency and then review briefly the multifractal framework. Second, we will introduce an innovative objective technique for determining if two stochastic processes can be regarded as being independent or not, and for investigating the nature of their potential coupling. Finally, we provide

some illustrative case studies demonstrating how these multifractal formalisms can improve our understanding of the structures and functions in marine systems.

Intermittency

The concept of intermittency has been initially described in the framework of turbulence, where experimental records of the kinetic energy dissipation rate ε showed strong and unpredictable bursts instead of a steady behavior of the fluctuations (Fig. 1). It has thus been known for a long time that the assumption of a spatially uniform turbulent cascade used by *Kolmogorov* (1941) is not satisfied for the increments of turbulent velocity at distances in the inertial subrange or shorter, and that strong gradients are more common than they would be for a Gaussian distribution (*Batchelor and Townsend*, 1949). This means that most of the time the gradients would still be of the order of their standard deviation, but that occasionally we should expect stronger burst, much more often than in the Gaussian case. This is the phenomenon of intermittency, which, as with other turbulent phenomena, is found at all scales.

This may be understood from a geometrical point of view considering that the turbulent regions do not fill the whole space, but only a subpart, in a very irregular way. This erroneous picture of a non-space filling turbulence takes the intermittent nature of turbulence into account by assuming that subeddies in the inertial subrange are either 'dead' (inactive) or 'alive' (active), and leads to a (mono-) fractal description of turbulence. However, it is now known that both turbulent velocity and passive scalars fluctuations are intermittent in the sense that strong (i.e. 'more active') subeddies occupy tiny fractions of the space available. This led to a multifractal description of turbulence, each intermittency level being associated with its own fractal dimension [see *Frisch* (1995) for more details].

In the following we quickly review how to characterize the statistics of a multifractal intermittent field.

Investigating single intermittent distributions: a brief review of the multifractal framework

Spectral analysis has been widely used in ecology to separate and measure the amount of variability occurring at different wavenumbers. In particular, assuming local isotropy and three-dimensional homogeneity of turbulence in the inertial subrange, the velocity fluctuations and the fluctuations of a passive scalar quantity P can be described in Fourier space by the spectral densities $E_V(k)$ and $E_P(k)$:

$$E_V(k) \propto k^{-\beta_V} \tag{1}$$

$$E_P(k) \propto k^{-\beta_P} \tag{2}$$

where k is a wavenumber, and with $\beta_V = \beta_P = 5/3$ for a non-intermittent turbulence (*Kolmogorov*, 1941; *Obukhov*, 1941,1949; *Corrsin*, 1951). However, spectral analysis and related techniques are implicitly based on Gaussian hypothesis untenable in an intermittent framework (*Seuront et al.*, 1999, 2001a). Thus, while random variability has been often modeled in marine ecology in the Gaussian framework, through, e.g., Gaussian distributions and Brownian motion (e.g., *Yamazaki and Okubo*, 1995; *Visser*, 1997), we will here generalize this approach fully taking into account the intermittency of turbulent velocity and passive scalar fluctuations.

Under fairly general conditions, the probability distribution of a random variable X is equivalently specified by its statistical moments. Here we consider the moments of the increments of a random field at all scales; this corresponds to the introduction of the structure functions exponents $\zeta_V(q)$ and $\zeta_P(q)$, which describe the multiscaling of the statistical moments of order q of turbulent velocity and passive scalar fluctuations:

$$\left\langle (\Delta V_l)^q \right\rangle \propto l^{\zeta_V(q)} \tag{3}$$

$$\left\langle (\Delta P_l)^q \right\rangle \propto l^{\zeta_P(q)} \tag{4}$$

where l is the spatial scale and the angle brackets "$\langle . \rangle$" indicate ensemble averaging. For monoscaling (i.e., monofractal) processes, the function $\zeta(q)$ is linear: $\zeta(q) = q/2$ for Brownian motion, and $\zeta(q) = q/3$ for Kolmogorov-Obukhov-1941. For multiscaling processes, this exponent is non-linear and concave.

While the functions $\zeta_V(q)$ and $\zeta_P(q)$ could depend on a very large number of parameters (a priori an infinite number of both integer and non-integer values of q), in the framework of universal multifractals they can be determined by only three parameters, with the general form $\zeta(q) = Aq + Bq^{\alpha}$ (*Schertzer and Lovejoy*, 1987). For turbulent velocity, the normalization conditions corresponding to the conservation of turbulent kinetic energy within the inertial subrange give $\zeta_V(3) = 1$, so that the resulting function can be written as

$$\zeta_V(q) = \frac{q}{3} - \frac{C_{1\varepsilon}}{\alpha_\varepsilon - 1}\left(\left(\frac{q}{3}\right)^{\alpha_\varepsilon} - \frac{q}{3}\right). \tag{5}$$

For a passive scalar P, there is no such a relation, and we

must keep three parameters, writing the expression as (*Seuront et al.*, 1996a, b, 1999, 2001a)

$$\zeta_P(q) = qH - \frac{C_{1P}}{\alpha_P - 1}\left(q^{\alpha_P} - q\right). \qquad (6)$$

H is the degree of non-conservation of the average process: $H = 0$ for a conservative process (i.e., scale-independent) and $H \neq 0$ for a non-conservative process (i.e., scale-dependent). H is given by $H = \zeta_P(1)$, while it can be seen from Eq. (5) that $\zeta_V(1) > 1/3$. C_1 is the codimension that characterizes the intermittency of the process and satisfies $0 \leq C_1 \leq d$ (d is the dimension of the observation space): $C_1 = 0$ for a homogeneous process, and C_1 increases with the intermittency of the process, indicating that the field values corresponding to any given level of variability are more scarce. The Lévy index α is the degree of multifractality, bounded between $\alpha = 0$ and $\alpha = 2$, corresponding to the monofractal case and to the maximum, or log-normal, multifractal case, respectively.

In other words, the second terms of Eqs. (5) and (6) express the multifractal intermittent deviation from monofractality, in which case $\zeta_V(q) = q/3$ and $\zeta_P(q) = qH$. The "distance" between monofractality and multifractality is then a function of C_1 and α. The knowledge of these parameters is enough to characterize all the one-point statistics of the fields. In particular, we see from Eqs. (5) and (6) that C_1 is given by $C_{1\varepsilon} = 1 - 3\zeta'_\varepsilon(3)$ for velocity fluctuations, and $C_{1\varepsilon} = H - \zeta'_P(1)$ for a passive scalar quantity P. α and α are estimated as the best nonlinear fit of Eqs. (5) and (6) for values between 0 and 2, using a simplex procedure.

Finally, we note here that in the multiscaling framework, intermittency is taken into account noting that

$$\beta_V = 1 + \zeta_V(2) \qquad (7)$$

$$\beta_P = 1 + \zeta_P(2). \qquad (8)$$

We thus see that the intermittency corrections introduced by the second term of Eq. (5) lead to $\beta_V > 5/3$. Furthermore, in order to conduct direct quantitative comparisons between the velocity and passive scalar intermittent corrections associated to C_1 values, let us note that the coefficients in front of the non-linear terms in Eqs. (5) and (6) are similar only if we compare C_{1V} and C_{1P}, with C_{1V} estimated as (*Schmitt et al.*, 1996; *Seuront et al.*, 1996a)

$$C_{1V} = 3^{-\alpha_\varepsilon} C_{1\varepsilon}. \qquad (9)$$

Investigating joint intermittent distributions: the "Generalized Correlation Functions"

Previous standard procedures devoted to test for independence between two given processes were generally based on second order statistics (i.e., covariance and correlation functions), even when they were conducted in scaling framework related to spectral analysis (*Legendre and Legendre*, 1984) or geostatistical analysis (*Kitanidis*, 1997). More recent procedures are based on probability density functions examination (*Lueck and Wolk*, 1999). The former are implicitly based on Gaussian hypothesis (uncorrelation implying independence), untenable in an intermittent framework characterized by a high-order statistical behavior. The latter do not deal with the intrinsic multiscaling properties of intermittent fields. We then propose here an original testing procedure based on a high-order generalization of the correlation concept between two variables X and Y.

Instead of random variables X and Y, we consider here two stochastic processes ΔX_l and ΔY_l (e.g., *Parzen*, 1962). For more convenience, let us note $x = \Delta X_l = e^{G_1}$ and $y = \Delta Y_l = e^{G_2}$. The joint moments can be written as the moments of a vectorial process:

$$\left\langle x^p y^q \right\rangle = \left\langle e^{pG_1 + qG_2} \right\rangle = \left\langle e^{\vec{Q}.\vec{G}} \right\rangle \propto l^{S(\vec{Q})} \qquad (10)$$

where the vectors $\vec{Q}$ and $\vec{G}$ are given by $\vec{Q} = (p,q)$ and $\vec{G} = (G_1, G_2)$, and the exponents $S(\vec{Q})$ characterize the multiscaling properties of the joint moments $\left\langle x^p y^q \right\rangle$. The "Generalized Correlation Function" (GCF hereafter) we introduce is then simply a normalization of the joint moments following:

$$c(p,q) = \frac{\left\langle x^p y^q \right\rangle}{\left\langle x^p \right\rangle \left\langle y^q \right\rangle} \propto l^{-r(p,q)}. \qquad (11)$$

The "Generalized Correlation Exponent" (GCE hereafter), estimated as the slope of the linear trend of $c(p,q)$ vs. l in a log-log plot, is then expressed as

$$r(p,q) = \zeta_X(p) + \zeta_Y(q) - S(p,q) \qquad (12)$$

where $\zeta_X(p)$ and $\zeta_Y(q)$ characterize the multiscaling properties of the single fluctuations $\left\langle x^p \right\rangle$ and $\left\langle y^q \right\rangle$ as defined in Eqs. (3) and (4), and $S(p,q)$ characterizes the multiscaling properties of the joint fluctuations $\left\langle x^p y^q \right\rangle$, see Eq. (11). Both $c(p,q)$ and $r(p,q)$ are generalization of correlation functions. They express the correlation between

x^p and y^q and their scale and moment dependence. In the particular case $p=q=1$, Eq. (11) recovers the classical expression of the correlation coefficient between x and y. We nevertheless need to emphasize here that, whereas independence implies uncorrelation, uncorrelation does not imply independence.

Indeed, uncorrelation corresponds simply to the relation $r(1,1)=0$. Uncorrelation implies independence only in special cases such as for Gaussian processes. To show this, let us consider the joint scaling function for lognormal multifractals x and y. Using results for multivariate Gaussian processes (see any text book on multivariate stochastic processes, e.g., *Samorodnitsky and Taqqu*, 1994), one has the general expression for a lognormal process:

$$S(p,q)=a_1p+a_2q-a_3q^2-a_4p^2-\sigma pq \qquad (13)$$

so that

$$r(p,q)=S(p,0)+S(0,q)-S(p,q) \qquad (14)$$

giving

$$r(p,q)=\sigma pq\,. \qquad (15)$$

In this case, it is clear that $r(1,1)$ or $r(2,2)$ is enough to estimate the only parameter, namely the correlation coefficient σ, so that if $r(1,1)=0$ or $r(2,2)=0$ it can be concluded that the two processes are independent. In the general case, this is no more true: independence between the stochastic processes x and y means that the GCE verifies $r(p,q)=0$ whatever the values of p and q, while uncorrelation corresponds to $r(1,1)=0$.

A function related to our $c(p,q)$ has also been independently introduced in the lognormal multifractal framework for financial time series by *Muzy et al.* (2000), where it was called "joint scaling exponent".

The function $c(p,q)$ and its related scaling exponent $r(p,q)$ can be used as an analysis tool to study some complex relationship between two multifractal fields x and y. To provide some basis for discussion and interpretation of experimental results, let us consider some limit cases.

If x and y are independent, as was said above, $r(p,q)=0$. On the other hand, in case of perfect proportionality $x=K.y$, where K is a constant, or for "random proportionality" $x=\kappa.y$, where κ is a random variable independent on y, it is readily seen that

$$r(p,q)=\zeta_Y(p)+\zeta_Y(q)-\zeta_Y(p+q)\,. \qquad (16)$$

In particular, one may note that $r(p,q)>0$ due to the convexity of the scaling functions $\zeta(p)$. This relation can be directly tested to verify the random proportionality hypothesis. Furthermore, the shape of the surface obtained is symmetric in the *p-q* plane.

Other simple situations may be considered: if $x=K.y^b$ with $b>0$ and K constant, or if $x=\kappa.y^b$ with κ random and independent of y, then one has

$$r(p,q)=\zeta_Y(bp)+\zeta_Y(q)-\zeta_Y(bp+q)\,. \qquad (17)$$

Eq. (17) is still positive, but no more symmetric in the *p-q* plane; it is symmetric in the *bp-q* plane. In this framework, the value of b may be first estimated as the positive value such that

$$r(p,0)=r(0,bp) \qquad (18)$$

Using the value estimated this way, this framework is then tested by verifying that $r(p/b,q)$ is indeed symmetric in the p-q plane. More generally speaking, the more $r(p,q)$ is positive, the more the $x=\Delta X_l$ and $y=\Delta Y_l$ are dependent random variables.

The main advantages of this framework are the following: (i) it makes no assumptions about the spectrum or the distribution of either data sets; (ii) it takes fully into account their intrinsic multiscaling properties; (iii) it may be used to provide much more fundamental relations between two patterns/processes; and iv) more generally it fully explores qualitatively and quantitatively the correlations of the fields x^p and y^q, revealing the correlations of large and low fluctuations of both processes.

Turbulent velocity fields

Turbulence measurements

Laboratory experiments

Turbulence has been generated by means of fixed PVC grids (diameter 2 mm, mesh size 1 cm) in a circular flume. Considering the dimensions of the flume and the flow velocities considered in the experiment (Table 1), we were dealing with a fully developed turbulence. A high-frequency (100 Hz) time series of instantaneous horizontal turbulent velocity was measured by hot-film velocimetry 10 and 20 cm behind the grid. The average turbulent energy dissipation rate was derived following the isotropic formula (*Tennekes and Lumley*, 1972):

$$\varepsilon=15\nu\int_{k_{min}}^{k_{max}}k^2E(k)\mathrm{d}k \qquad (19)$$

where ε is the turbulent energy dissipation rate (m^2s^{-3}), k the wavenumber ($k=2\pi/\lambda$, m^{-1}), λ the eddy wave-

length (m), k_{min} and k_{max} respectively the smallest and largest wavenumber resolved, and $E(k)$ the turbulence spectrum (m s^{-2}). The spectrum $E(k)$ is regarded as the mean-square amplitude of velocity fluctuations associated with a wavenumber of turbulent motion.

Table 1. Main characteristics of the grid-generated turbulence experiment (*d*: distance from the grid; *Re*: Reynolds number; *N*: numbers of time series analyzed).

d (cm)	Speed (m s^{-1})	ε (m^2 s^{-3})	*Re*	*N*
20 cm	0.15	$2.86\ 10^{-8}$	$45\ 10^3$	5
	0.20	$3.54\ 10^{-6}$	$60\ 10^3$	5
	0.25	$9.14\ 10^{-6}$	$75\ 10^3$	5
	0.30	$1.36\ 10^{-5}$	$105\ 10^3$	5
	0.35	*1.64 10^{-5}*	$105\ 10^3$	5
	0.40	$1.82\ 10^{-5}$	$120\ 10^3$	5
10 cm	0.15	$1.01\ 10^{-7}$	$45\ 10^3$	4
	0.20	$1.24\ 10^{-5}$	$60\ 10^3$	5
	0.25	$3.2\ 10^{-5}$	$75\ 10^3$	5
	0.30	$4.75\ 10^{-5}$	$105\ 10^3$	5
	0.35	$5.75\ 10^{-5}$	$105\ 10^3$	5
	0.40	$6.36\ 10^{-5}$	$120\ 10^3$	5

To investigate potential differences in the structure of velocity fields in relation to the different levels of the turbulent kinetic energy, we analyzed here 5 time series of 1 min duration (i.e., 6000 data points) for 5 flow velocities at the two locations considered behind the grid.

Field experiments

Measurements of the turbulence fields were done using TurboMAP (Turbulence Ocean Microstructure Acquisition Profiler), a free-fall integrated system housed in an HCR treated aluminum pressure case, specifically designed for concurrent measurements of turbulent parameters (shear, $\partial u/\partial z$, where u and z are the turbulent fluctuating cross-stream velocity component and the depth, respectively), hydrographic parameters (pressure, temperature and conductivity) and bio-optical parameters (*in vivo* fluorescence and backscatter). All sensors are set into a parabolically shaped cap at the top of the pressure case. This arrangement ensures that these sensors point into an undisturbed flow. All signals are simultaneously sampled at 256 Hz and stored internally in a PCMCIA memory card. More details on the description and evaluation of both design and performance of this instrument can be found in *Wolk et al.* (2001 a,b).

In this paper, we focus only on the ability of this new high-resolution biophysical profiler to measure the shear signal, $\partial u/\partial z$. In that way, we use 8 vertical shear profiles, recorded on 21 August 1998 in a tidal channel located between Neko-Seto and Meneko-Seto Straits (Japan). The sampling location has been chosen because this area is characterized by very strong tidal currents (up to 180 cm s^{-1}), associated with channel narrowing, and a subsequent high tidal mixing (*Takasugi et al.*, 1994a, b).

The turbulent velocity fluctuations are measured with a standard piezo-ceramic shear probe, which has extensively been described elsewhere (e.g., *Lueck et al.*, 1997). The probe is associated with three orthogonal accelerometers mounted inside the pressure case and is used to quantify noise level of velocity shear and to clean the shear signal of possible narrow-band contaminations from vehicle vibrations (*Levine and Lueck*, 1999).

To recover the turbulent fluctuating velocity u from $\partial u/\partial z$, we run an anti-derivative digital filter over the shear data, which consists of a scaled single-pole low-pass filter with a cut-off frequency f_c. The f_c is a function of the integration time scale t_i as $f_c = 1/2.3t_i$ [see *Wolk and Lueck* (2001) for further details]. Here we used $t_i = 7.5$ s and $f_c = 0.06$ Hz, leading to a maximum wavelength resolved to 10 m. The lowest frequency resolved is determined by the high-pass filtering of the shear probe signal to minimize pyro-electric effects (70 Hz).

The vertical distribution of the turbulent kinetic energy dissipation rates ε has been estimated, after systematic denoising and despiking, from shear power spectra computed for 512 successive segments of shear (i.e., every meter considering an average profiler sinking velocity of 0.5 m s^{-1}) following the isotropic formula defined above in Eq. (19).

Considering the extreme fluctuations observed in the vertical distribution of the dissipation rates ε (Fig. 1), our analysis has been conducted on all the 512 data point segments available within each vertical profile (Table 2).

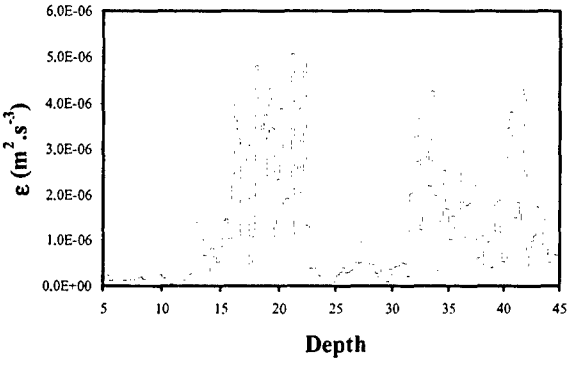

Figure 1. Example of the intermittent character of the vertical distribution of the kinetic energy dissipation rate ε, which has been estimated every meter using Eq. (19).

Table 2. Depth, numbers of 512 data points subsections, and mean of the turbulent kinetic energy dissipation rate ε ($m^2 s^{-3}$), for each of the eight vertical profiles.

Data set	N	n	ε
1	14463	28	$1.80\ 10^{-8}$
2	20479	40	$1.87\ 10^{-7}$
3	21887	43	$6.98\ 10^{-8}$
4	18431	36	$6.43\ 10^{-8}$
5	10495	20	$9.61\ 10^{-8}$
6	22911	45	$1.33\ 10^{-6}$
7	29949	58	$3.72\ 10^{-7}$
8	17279	34	$5.65\ 10^{-8}$

Characterizing turbulent velocity fields

The velocity spectra exhibit a scaling behavior ranging between 0.185 ± 0.1 m and 0.013 ± 0.015 m for velocity fluctuations measured in our circular flume, and between 1.0 ± 0.1 m and 0.050 ± 0.005 m for the velocity fluctuations estimated from shear data recorded in the field (Fig. 2). These scaling behaviors are qualitatively close (we try a quantification later) to the theoretical –5/3 Kolmogorov's power law over roughly 1.1 and 1.3 decades, respectively, with $\beta_V \approx 1.70$ in both cases. The ranges of scales defined that way will be regarded as the inertial subrange.

The estimates of the velocity structure functions $\langle (\Delta V_l)^q \rangle$ confirm the scaling regimes previously shown by spectral analysis for different orders of moment q (Fig. 3). Estimated scale ratios, highest and lowest wavenumbers of scaling ranges observed for the 512 data points subsections considered within each profile, exhibit very similar patterns to those observed in the spectral framework. We refer the reader to Table 1 for further details. We subsequently computed the scaling exponents $\zeta(q)$ for several values of q between 0 and 10 (i.e. with 0.1 increments) for the range of scales where $\zeta_V(3) = 1$ is valid; this range of scales characterizes here the inertial subrange. The scaling of the second-order moments $\zeta_V(2)$ confirms the estimates of the spectral exponents β_V [$\beta_V = 1 + \zeta_V(2)$, Eq. (7)]: $\zeta_V(2) = 0.710 \pm 0.010$ for grid-generated turbulence and $\zeta_V(2) = 0.705 \pm 0.005$ for ocean turbulence.

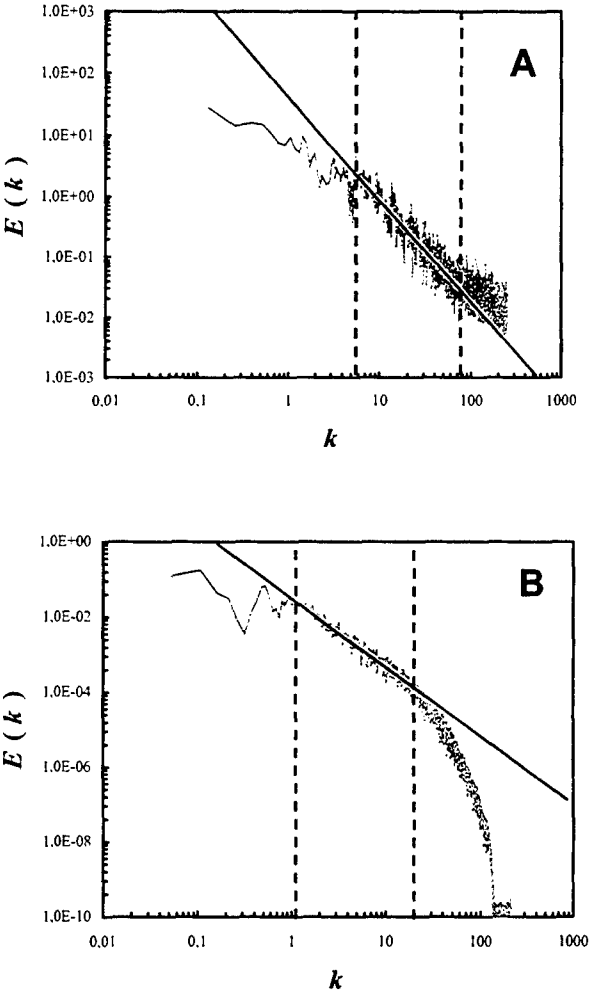

Figure 2. Samples of the power spectral density $E(k)$ of turbulent velocity fluctuations recorded with a hot-film velocimeter (A) located behind a grid in a circular flume, and (B) in a tidally mixed tidal channel, shown in log-log plots as a function of the wavenumber k (m^{-1}). The vertical dotted lines indicate the inertial subrange over which the spectra roughly follow the power-law form $E(k) \propto k^{-\beta_V}$, with $\beta_V \approx 5/3$ (continuous lines).

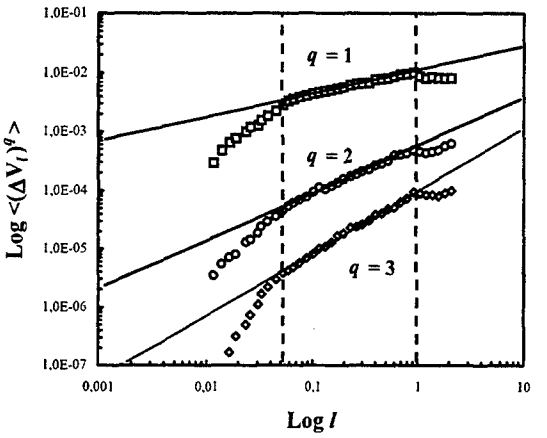

Figure 3. The velocity structure functions $\langle(\Delta V_l)^q\rangle$ of ocean velocity versus the length scale l in a log-log plot for various values of the statistical order of moment q (i.e., q = 1, 2 and 3, from top to bottom). Linear trends are clearly visible, whatever the order of moment q (continuous lines), and indicate the multiscaling nature of our datasets. The vertical dotted lines correspond to the upper and lower limits of the inertial subrange. Note that the different scaling ranges (estimated from the profile shown in Fig. 2a) are indistinguishable from the one estimated from spectral analysis.

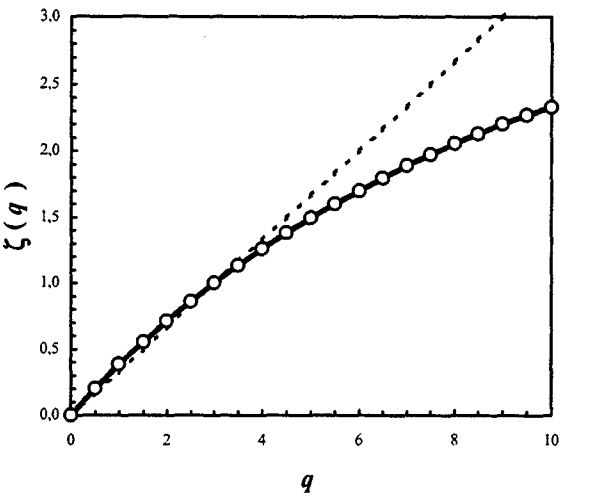

Figure 4. The scaling exponents structure function $\zeta_V(q)$ empirical curves (open dots) estimated from grid-generated turbulent velocity fluctuations, compared to the monofractal curve $\zeta_V(q)=q/3$ (dashed line), and to the universal multifractal curve (thick continuous curve) obtained with $C_{1\varepsilon}=0.18$ and $\alpha_\varepsilon=1.52$ in Eq. (5).

More generally, the clear nonlinearity of the functions $\zeta_V(q)$ (Fig. 4) is direct evidence for the multifractal nature of the velocity fluctuations. Moreover, within experimental error, the functions $\zeta_V(q)$ for grid-generated and ocean turbulent velocity fluctuations cannot be qualitatively shown as being different. While the similarity observed in the shape of the functions $\zeta_V(q)$ qualitatively suggests some convergent behavior in the high-order structure of velocity fluctuations, the values of the universal multifractal parameters $C_{1\varepsilon}$ and α_ε lead to specifying these results. These parameters have been estimated as $C_{1\varepsilon}=0.18\pm0.02$, and $\alpha_\varepsilon=1.52\pm0.03$ for grid-generated turbulence, and $C_{1\varepsilon}=0.16\pm0.02$ and $\alpha_\varepsilon=1.55\pm0.04$ for ocean turbulence. That leads to confirmation that the structure of velocity fluctuations recorded in the field and in the laboratory cannot be regarded as being significantly different.

On the other hand, the parameters C_{1V}, estimated using $C_{1\varepsilon}$ and α_ε in Eq. (9) as $C_{1V}=0.032\pm0.02$, appear slightly smaller than the values reported in the literature for the parameters C_{1P} characterizing the intermittent behavior of temperature and salinity in highly dissipative areas: $C_{1T}\in[0.035-0.060]$ and $C_{1S}\in[0.035-0.062]$ (*Seuront et al.*, 1996a,b, 1999, 2001a). This implies that the temperature and salinity fields are much more intermittent than the velocity field; this high intermittency can be related to the strong discontinuities ("ramps") observed in the temperature signals (*Sreenivasan*, 1991; *Pumir*, 1994b). Intermittency for passive scalars, in both two and three dimensions, has also been studied in direct numerical simulations (*Holzer and Siggia*, 1994; *Pumir*, 1994a,b). Such simulations often reveal extended regions of almost uniform temperature separated by boundary layers (ramps) with strong gradients.

We should finally note that the multifractal parameters $C_{1\varepsilon}$ and α_ε obtained here for the very first time for oceanic turbulence are very similar to the parameters estimated for atmospheric turbulence: $C_{1\varepsilon}=0.15\pm0.03$ and $\alpha_\varepsilon=1.50\pm0.05$ (Fig. 5; *Schertzer et al.*, 1995; *Schmitt et al.*, 1992a, b, 1993, 1996; *Chigirinskaya et al.*, 1994). As previously noticed by *Seuront et al.* (2001b), these results suggest a strong similarity of the intermittent nature of turbulent velocity fluctuations in the atmosphere and the ocean. The resolution of this particular issue, well beyond the scope of the present paper, is in progress. In particular, the question is whether atmospheric and oceanic temperature fields behave in a similar fashion (*Seuront and Yamazaki*, 2001; *Seuront et al.*, 2001c).

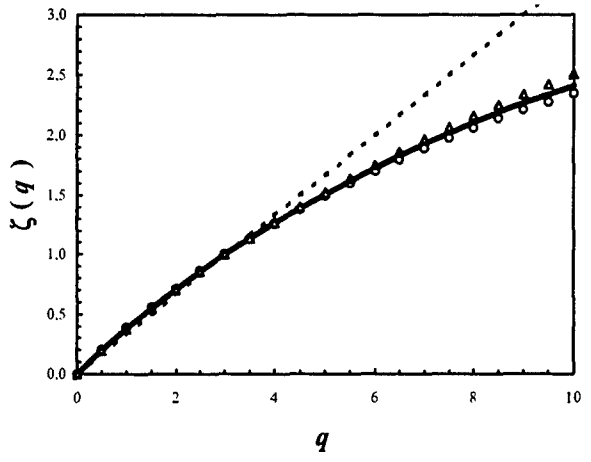

Figure 5. Comparison of the empirical values of the functions $\zeta_V(q)$ estimated from grid generated turbulence (open dots) and field ocean turbulence (open triangles), with the universal multifractal fit obtained with $C_{1\varepsilon}$ and α_ε values characteristic of atmospheric turbulence, i.e. $C_{1\varepsilon}=0.15$ and $\alpha_\varepsilon=1.50$ in Eq. (5). The linear curve $\zeta_V(q)=q/3$ expected in case of non-intermittent turbulence is shown for comparison (dashed line).

Ocean passive and "biologically active" scalars

Phytoplankton of the Eastern English Channel

In a recent paper, *Seuront et al.* (1999) showed that the small-scale intermittent distribution of temperature (a scalar quantity passively advected by turbulent fluid motions) and phytoplankton biomass recorded in the coastal waters of the Eastern English Channel were indistinguishable, both in spectral and multifractal framework (Fig. 6). They subsequently concluded their study stating that phytoplankton biomass could be regarded as a purely passive scalar at small scales. Here, small scales correspond to temporal scales bounded between 1 and 20 seconds. Using the Taylor's theory of frozen turbulence, these temporal scales can be related to spatial scales bounded between 0.1 and 22 meters. For larger scales, the phytoplankton biomass exhibits a very specific heterogeneous distribution, dominated by biological processes resulting from complex interactions between the turbulence level of fluid motions (mainly different tidal conditions related to both ebb/flood and neap/spring tidal cycles), the phytoplankton biomass concentration, and the specific composition of phytoplankton assemblages (*Seuront et al.*, 1996b; *Seuront et al.*, 1999). These larger scales are not investigated in the present work.

Table 3. Mean values of the empirical estimates of the spectral exponent β_F, and the universal multifractal parameters H_F, C_{1F} and α_F for subsets of *in vivo* fluorescence time series recorded under different levels of turbulence.

ε ($m^2.s^{-3}$)	β	H	C_1	α
$1\ 10^{-6}$	1.76	0.43	0.060	1.80
$5\ 10^{-6}$	1.76	0.43	0.055	1.82
$1\ 10^{-5}$	1.77	0.42	0.050	1.80
$5\ 10^{-5}$	1.78	0.42	0.045	1.81
$1\ 10^{-4}$	1.78	0.41	0.040	1.80

Turbulence and phytoplankton patchiness

Considering the role played by turbulence in the formation and disruption of particle aggregates [e.g., *Kiørboe* (1997) and references therein], and the highly varying dissipation rates of turbulent energy observed over a tidal cycle in this area (between 10^{-6} and 10^{-4} $m^2\ s^{-3}$; *Seuront et al.*, 2001a), the question here is whether the local hydrodynamic conditions have an effect on both temperature and phytoplankton biomass local distributions.

The original 46 h 24 min time series recorded at 1 Hz (i.e., 167040 data; *Seuront et al.*, 1999) has then been divided into 46 subseries of 1 h (i.e., 3600 data). We then built 5 sets of 7 subseries, each set corresponding to a different level of dissipation rates ranging from $\varepsilon=10^{-6}$ $m^2.s^{-3}$ to $\varepsilon=10^{-4}$ $m^2.s^{-3}$. We then conducted both spectral and multifractal analyses on each subseries of temperature and *in vivo* fluorescence within a given subset, and the resulting observations led to different comments (Table 3).

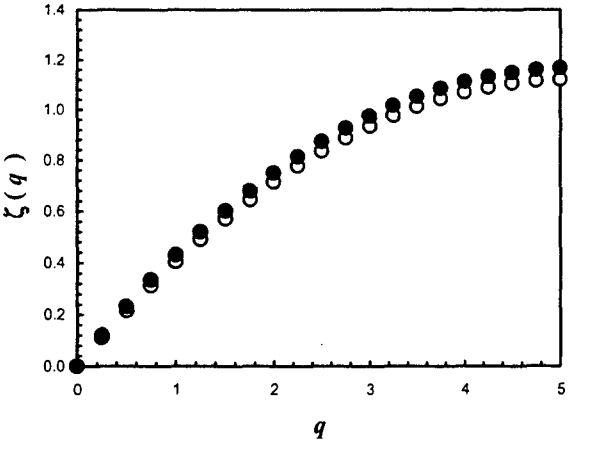

Figure 6. Comparison of the functions $\zeta_T(q)$ (open dots) and $\zeta_F(q)$ (black dots) estimated from small scale (<20 seconds) temperature and *in vivo* fluorescence fluctuations; (adapted from *Seuront et al.*, 1999).

The slopes β_T and β_F, estimated for the frequency bands that maximized the coefficient of determination and minimized the total sum of squared-residuals for the regression in log-log plots of the temperature and fluorescence power spectra [cf. Eq. (2)], cannot be statistically distinguished within each set of temperature and fluorescence subseries (analyses of covariance, $p > 0.05$), nor between the 5 sets considered ($p > 0.05$). These results, fully congruent with previous studies conducted in the same area (*Seuront et al.*, 1996a, b, 1999, 2001a), suggest extreme similarity between the single scaling properties of small-scale temperature and fluorescence distributions. At this stage, phytoplankton biomass can then still be regarded as being a passive scalar.

The nonlinear behavior of the functions $\zeta(q)$ confirms and generalizes in different hydrodynamic regimes the multifractal nature of temperature and *in vivo* fluorescence observed by *Seuront et al.* (1999) using a global approach of the same data set (Fig. 6). However, the functions $\zeta_T(q)$ obtained for temperature time series remain similar whatever the external hydrodynamic forcing (i.e., the values of the dissipation rate ε), while the nonlinearity (i.e., convexity) of the functions $\zeta_F(q)$ characterizing phytoplankton biomass clearly increases when the value of the dissipation rate ε decreases (Fig. 7).

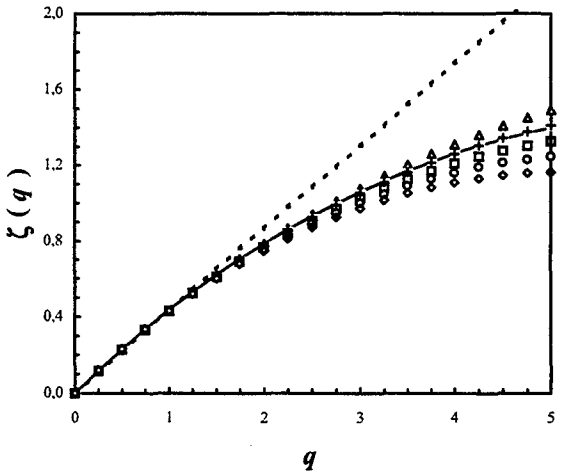

Figure 7. Comparison of the empirical values of the functions $\zeta(q)$ estimated for temperature (continuous curve) and *in vivo* fluorescence for different values of the turbulent kinetic energy dissipation rate ε ($\varepsilon = 10^{-6}$ m^2 s^{-3}, rhombs; $\varepsilon = 5\times10^{-6}$ m^2 s^{-3}, circles; $\varepsilon = 10^{-5}$ m^2 s^{-3}, squares; $\varepsilon = 5\times10^{-5}$ m^2 s^{-3}, crosses; $\varepsilon = 10^{-4}$ m^2 s^{-3}, triangles). The linear curve $\zeta_T(q) = qH$ expected in case of non-intermittent turbulence in shown for comparison (dashed line).

The distribution of temperature then remains the same whatever the hydrodynamic conditions. This result is convergent with our previous observations regarding the distribution of turbulent velocity fields, and it confirms the passive scalar behavior of temperature.

On the other hand, the distribution of phytoplankton biomass is less intermittent and is closer to that of temperature in high turbulent conditions (Fig. 7). This suggests that phytoplankton cells behave more like a passive scalar under high hydrodynamic conditions but exhibit very specific properties under lower levels of turbulence.

The universal multifractal parameters H, C_1, and α confirm these qualitative observations (Table 3). Let us remember here that the parameters H, C_1, and α have been obtained by fitting the universal multifractal model detailed in Eq. (6) to the empirical function $\zeta(q)$ as described above. These parameters remain constant for temperature time series with $H_T = 0.40$, $C_{1T} = 0.05$ and $\alpha_T = 1.90$. On the other hand, it is shown that only H and C_1 remain roughly constant for fluorescence, with $H_F = 0.42 \pm 0.01$ and $\alpha_F = 1.81 \pm 0.01$ [values compatible with the $H_F = 0.43$ and $\alpha_F = 1.80$ found by *Seuront et al.* (1999)]. However, the parameter C_{1F} is highly variable. It increases 33% when the dissipation rate ε decreases from the highest to the lowest values experienced over a tidal cycle, i.e. from $\varepsilon = 10^{-4}$ to $\varepsilon = 10^{-6}$ m^2.s^{-3}. Under low hydrodynamic conditions the higher values of C_{1F} indicate the occurrence of few patches of high phytoplankton concentrations that are several orders of magnitude above background levels. Under higher hydrodynamic conditions the lower values of C_{1F} indicate that phytoplankton cells are more homogeneously distributed and behave as a passive scalar. Here the so-called homogenization effect is thought to be associated with the disruption of these phytoplankton patches. This hypothesis is supported by the C_{1F} values observed for fluorescence time series under high hydrodynamic conditions, which cannot be distinguished from the C_{1F} values estimated for temperature irrespective of hydrodynamic conditions, and by the extreme similarity of the empirical functions $\zeta_T(q)$ and $\zeta_F(q)$ in high hydrodynamic conditions (Fig. 7).

Turbulence and biophysical couplings

In order to investigate the nature of the dependence between temperature and phytoplankton distributions, we subsequently computed the Generalized Correlation Functions, $c(p,q)$ and the related Generalized Correlation Exponents, $r(p,q)$, between temperature and fluorescence

time series, within each subset defined above.

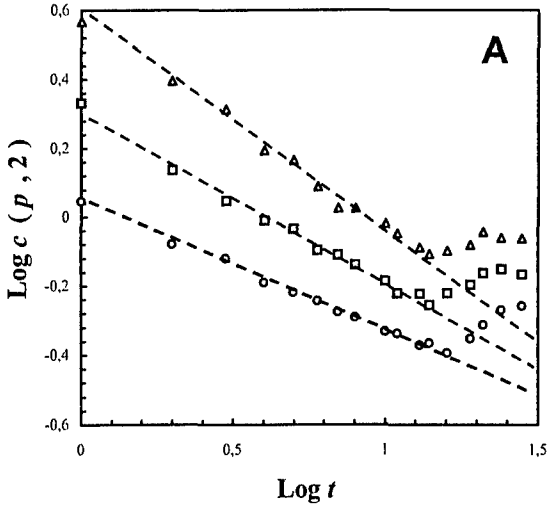

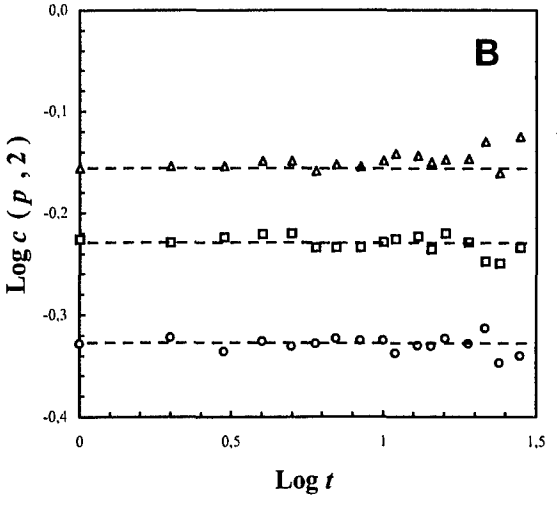

Figure 8. The Generalized Correlation Functions (GCF) $c(p,q)$ versus the time scale t in log-log plots, for (A) simultaneously and (B) independently sampled temperature and *in vivo* fluorescence time series. The function $c(p,q)$ shown here has been estimated for a constant value of the statistical order of moment q of temperature fluctuations ($q = 2$), and various values of the statistical order of moment p of *in vivo* fluorescence (i.e. p = 1, 2 and 3, from bottom to top). The slopes of the linear regression estimated over the scaling ranges (dashed lines) provide estimates of the Generalized Correlation Exponents (GCE) $r(p,q)$.

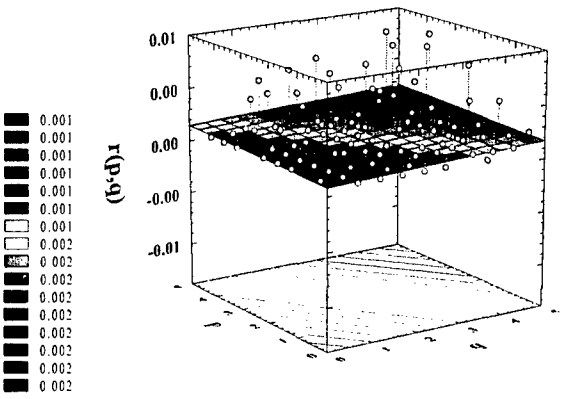

Figure 9. The Generalized Correlation Exponents (GCE $r(p,q)$, shown as a function of both p and q, which characterize *in vivo* fluorescence and temperature fluctuations, respectively. The function $r(p,q)$ is estimated here between time series of temperature and fluorescence independently sampled (C).

Figure 8 shows the GCF, $c(p,q)$, plotted in log-log plots versus the time scale t, for simultaneously recorded temperature and fluorescence time series (Fig. 8a), as well as for temperature and fluorescence time series taken at different moments of the tidal cycle, and *a fortiori* independent (Fig. 8b). Both the linear behavior of the functions $c(p,q)$ over scales ranging between 1 and 20 seconds, and the positive values taken by the GCE, $r(p,q)$, estimated as the slope of the linear trend of the GCF $c(p,q)$ vs. t in a log-log plot, whatever the combinations of p and q values (Fig. 8a) confirm the validity of Eq. (11). On the other hand, the weak values taken by the functions $c(p,q)$ estimated between independent temperature and fluorescence time series (Fig. 8b) indicate a low correlation between the temperature and phytoplankton biomass fluctuations, $\left\langle (\Delta T_l)^q \right\rangle$ and $\left\langle (\Delta F_l)^p \right\rangle$. This is confirmed by the related values of the functions $r(p,q)$, which remain close to zero, whatever the combinations of p and q values (Fig. 9).

We subsequently refined these observations, comparing the functions $r(p,q)$ obtained between temperature and fluorescence time series in different turbulent conditions. Figure 10 then shows the $r(p,q)$ obtained for all the combinations of p and q values with 0.1 increments, for three levels of turbulence (10^{-4}, 10^{-5} and 10^{-6} $m^2 s^{-3}$). It appears that the correlation between temperature and *in vivo* fluorescence fluctuations increases with hydrodynamic conditions and is weaker, even nil, in low turbulent conditions.

We confirm here the increased physical control suggested under strong turbulent conditions from the analysis of the shape of the function $\zeta_F(q)$, and its comparison

with the function $\zeta_T(q)$; see Figure 7. On the other hand, the decorrelation between temperature and phytoplankton fluctuations under weak turbulent conditions suggests an increase in the biological contributions to the control of phytoplankton biomass distribution, and confirms previous observations (cf. Fig. 7). Phytoplankton distribution then appears independent of the temperature distribution under the lowest turbulence levels investigated here, i.e., 10^{-4} m^2 s^{-3} (Fig. 10a).

More precisely, the shape of the function $r(p,q)$ indicates that large phytoplankton fluctuations are associated—under strong enough turbulent conditions—to weak temperature gradients, and conversely. This tendency seems to reflect, over a slightly wider range of scales, findings of *Desiderio et al.* (1993); they observed the occurrence of 0.1-0.2 meter thick fluorescent layers just above local temperature gradients. While these qualitative comments suggest a proportionality relationship between temperature and phytoplankton fluctuations, the relation (16) has never been verified. The phytoplankton fluctuations then cannot be regarded as strictly proportional or randomly proportional to the fluctuations of temperature, i.e., $\Delta F = K.\Delta T$ and $\Delta F = \kappa.\Delta T$, respectively. In contrast, the relation (17) has been verified testing the validity of Eq. (18) over a wide range of b values. Using b values ranging between 0.05 and 5 (with 0.05 increments), we then showed that Eq. (18) is verified for three of the five levels of turbulence investigated here: $\varepsilon = 10^{-4}$ $m^2 s^{-3}$ with $b = 2.69$, $\varepsilon = 5.10^{-4}$ $m^2 s^{-3}$ with $b = 2.25$, and $\varepsilon = 10^{-5}$ m^2 s^{-3} with $b = 1.76$. Figure 11 shows the relation $r(p,0)$ vs. $r(0,bp)$ corresponding to the functions $r(p,q)$ shown in Fig. 10b and c, with $b = 2.69$ and $b = 1.76$, respectively. The correlation shown between temperature and phytoplankton fluctuations under high turbulent conditions, is then related to a power-law dependence relationship, i.e. $\Delta F = \kappa.(\Delta T)^b$.

Let us mention here that at this stage of the development of the multiscaling techniques illustrated in the present paper, the presence and the absence of evidence for power-law dependence between phytoplankton and temperature fluctuations cannot (*a priori*) be regarded as a general rule driving biophysical couplings in pelagic ecosystems. Indeed, the relationship between temperature and in vivo fluorescence or, more generally, biophysical couplings, can be influenced, and then complexified, by both the processes related to phytoplankton cells ecology and to the sampling strategy. Over the range of scales investigated in the present study, *in vivo* fluorescence fluctuations can indeed result from nonlinear interactions between the physiological state of phytoplankton cells, their related coagulation ability, the specific composition of phytoplankton assemblages, the grazing impact of copepods

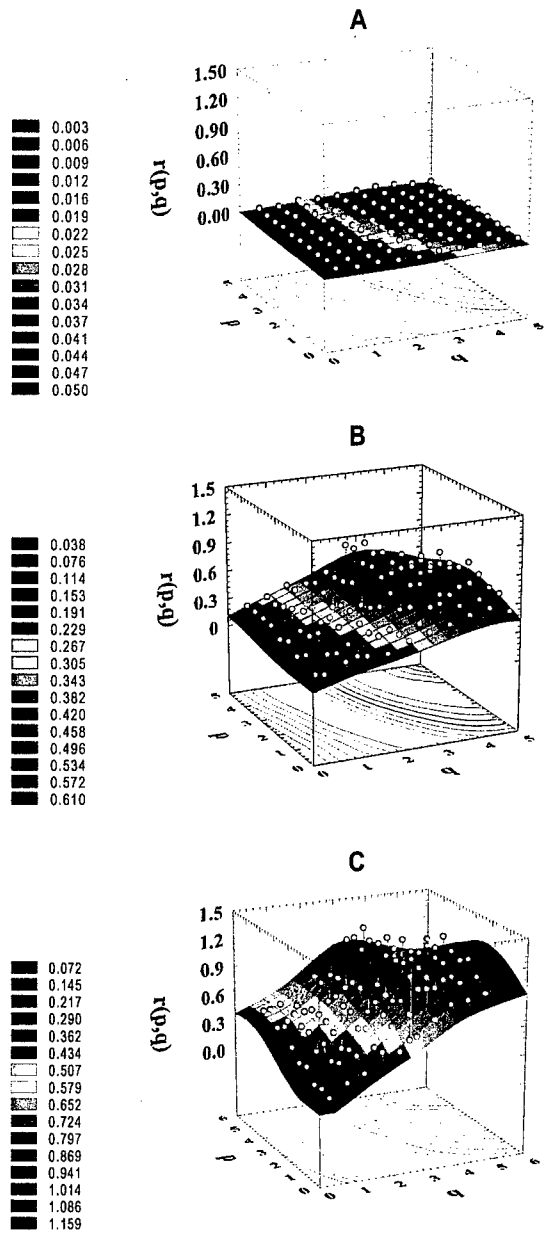

Figure 10. The Generalized Correlation Exponents (GCE $r(p,q)$, shown as a function of both p and q. Here the statistical orders of moment p and q characterize temperature and *in vivo* fluorescence fluctuations, respectively. The functions $r(p,q)$ correspond to three different levels of turbulence, i.e. (A) $\varepsilon = 10^{-6}$ (B), 10^{-5}, and (C) 10^{-4} $m^2 s^{-3}$.

(shown recently to influence both spectral and multifractal properties of phytoplankton biomass; *Seuront*, 1999; *Lovejoy et al.*, 2001), and the turbulent processes. The resulting fluctuations can then be potentially more complex than those observed for a purely passive scalar such as temperature.

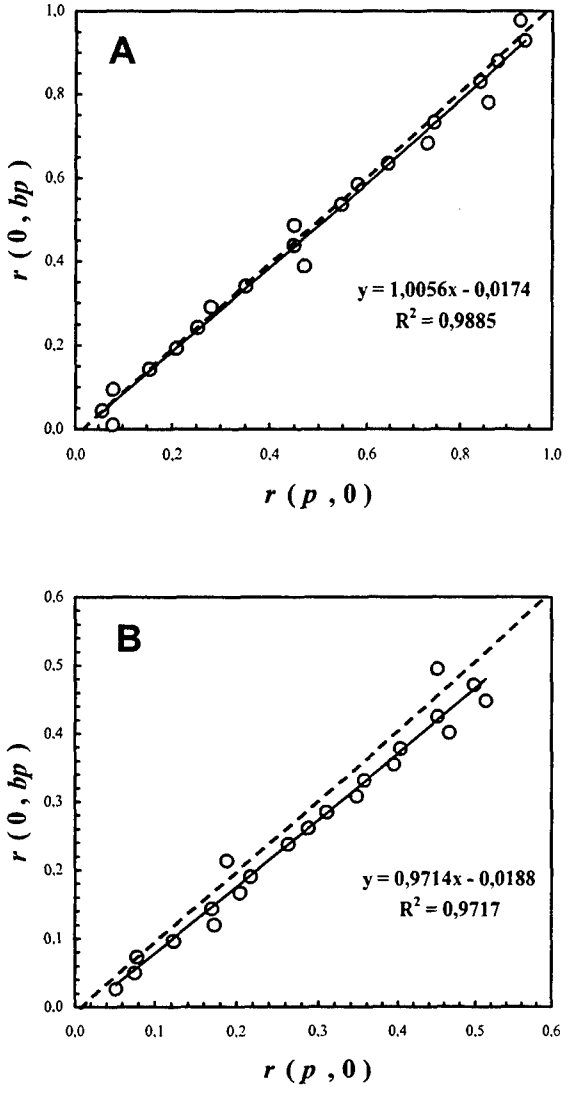

Figure 11. Plots of the Generalized Correlation Exponents $r(p,0)$ versus $r(0,bp)$ for two levels of turbulence, $\varepsilon = 10^{-4}$ with $b = 2.69$ (A) and $\varepsilon = 10^{-5}$ with $b = 1.76$ (B). The slopes of the regression lines (continuous line) cannot be distinguished from that of the relation $bp = q$ (dashed line). This shows the validity of Eq. (18) and the symmetry of the functions $r(p,q)$ in the $bp - q$ plane.

On the other hand, considering (i) the highly intrusive character of the sampling device used to record temperature and *in vivo* fluorescence (a Sea-Bird 25 Sealogger CTD probe and a Sea Tech fluorometer, respectively), and (ii) the spatial separation of the temperature and fluorescence sensors (≈10 cm), it is reasonable to think that the most extreme events, which are also the most infrequent and contribute to the highest values of the moments p and q, are not necessarily simultaneously sampled in a proper way, leading to spurious joint high-order properties. In particular, this could explain the weakening of the Generalized Correlation Exponents, $r(p,q)$, for values of the moments p and q such as $p \geq 4$ and $q \geq 4$. The latter limitation will be easily fixed in the near future with the increasing development and availability of microstructure profilers able to record both physical and biological parameters with a high-spatial resolution from mildly intrusive sensors (*Seuront et al.*, 2001d,e). The former limitation will be difficult to overcome, because of the intrinsic physiological, biological, and ecological processes affecting phytoplankton populations.

Conclusions: the cost and gain of increasing analysis complexity

Our results demonstrate that single scaling properties of temperature and phytoplankton would have erroneously led to conclude that the latter could be regarded as a purely passive scalar. However, investigations of their detailed variability in the universal multifractal framework lead to consideration that phytoplankton biomass presents very specific properties, depending on the intensity of local turbulent processes. This suggests a differential control of phytoplankton biomass distribution involving complex interactions between turbulent velocity fields and the involved particles properties such as buoyancy, size, density or aggregative properties. In particular, this assertion is supported by the specific behavior of phytoplankton multiscaling properties under low turbulent conditions, suggesting the prevalence of phytoplankton cells specific properties on turbulent processes.

This has been confirmed and specified by the introduction of the Generalized Correlation Functions/Exponents. The correlation—and then the couplings—between temperature and phytoplankton biomass fluctuations are thus higher under high hydrodynamic forcing and decrease progressively to collapse under low hydrodynamic forcing. In particular, careful examination of the functions $r(p,q)$ indicates that large phytoplankton fluctuations are associated—under strong enough turbulent conditions—with weak temperature gradients, and conversely. These results are fully congruent with more intuitive and qualitative results by *Desiderio et al.* (1993) over similar scales and *Wolk et al.* (2001) at smaller scales. Whatever that may be, even if additional work and data sets will be needed to achieve more definitive functional scenarios, the joint multifractal framework introduced here provides the first objective method to characterize, both qualitatively and quantitatively, the details of the relationships between any pair of simultaneously recorded patterns or processes. In

particular, this framework makes no assumptions about the spectrum or the distribution of either data sets, and it takes fully into account their intrinsic multiscaling properties. We should also note here that this work provides the very first evidence of the multifractal character of ocean turbulent velocity fluctuations, and reveals their extreme similarity in the ocean and the atmosphere.

Finally, regarding the additional quantity of information brought by the univariate and bivariate multiscaling procedures described here to our understanding of the structure of velocity, temperature and phytoplankton fluctuations, as well as of the couplings between temperature and phytoplankton biomass, we claimed, as already stressed elsewhere (e.g., *Yamazaki,* 1993; *Seuront,* 2001; *Seuront et al.*, 2001c), that taking into account the reality of the intermittent nature of bio-physical microstructures could be the first step towards a general understanding of structures and functions in marine pelagic ecosystems. The quite elevated cost associated with making use of the single and joint multifractal tools presented here in terms of algorithmic developments and computation time consumption will then be easily overcome by the priceless gain in emerging knowledge.

Acknowledgments. We are grateful to Prof. C. Garrett for his kind invitation to participate to the 'Aha Huliko'a winter workshop, and for his interest and constructive comments on the earliest version of this work. This work has been initiated while LS was a postdoctoral fellow granted by the Japan Society for the Promotion of Science (grant JSPS99756), and hosted by Prof. H. Yamazaki at the Tokyo University of Fisheries. We especially thank F. Wolk for his help in recovering the turbulent velocity from the shear signal and computing the dissipation rates, as well as for his highly stimulating conversation. We also greatly acknowledge Drs. F. Chavez, M.B. Matthews, J.G. Mitchell, R.G. Lueck, S. Souissi, PG Strutton and H. Yamazaki for constructive discussions about the GCF/GCE framework. We finally acknowledge all the participants of the 'Aha Huliko'a winter workshop for their stimulating scientific company, especially M. Barry, A. Mahadevan, A. Natarov, R. Ferrari, G. Holloway, D.L. Rudnick and W. Young.

References

Batchelor G.K., and A.A. Townsend, The nature of turbulent motion at large wavenumbers. *Proc. Roy. Soc. A, 199*, 238-250, 1949.

Chigirinskaya, Y., D. Schertzer, S. Lovejoy, A. Lazarev, and A. Ordanovich, Unified multifractal atmospheric dynamics tested in the tropics: horizontal scaling and self criticality. *Nonlinear Proc. Geophys., 1*, 105-114, 1994.

Corrsin, S., On the spectrum of isotropic temperature in an isotropic turbulence. *J. Appl. Phys., 22*, 469, 1951.

Cowles, T.J., R.A. Desiderio, and M.E. Carr, Small-scale planktonic structure: presistence and trophic consequences, *Oceanography, 11*, 4-9, 1998.

Desiderio, R.A., T.J. Cowles and J.N. Moum, Microstructure profiles of laser-induced chlorophyll fluorescence spectra: evaluation of backscatter and forward-scatter fiber-optic sensors, *J. Atmos. Oceanic Tech., 10*, 209-224, 1993.

Frish, U., Turbulence, Cambridge University Press, 1995.

Gibson, C.H., Kolmogorov similarity hypotheses for scalar fields: sampling intermittent turbulent mixing in the ocean and galaxy, *Proc. R. Soc. London A, 434*, 149-164, 1991.

Holzer, M,. and E.D. Siggia, Turbulent mixing of a passive scalar. *Phys. Fluids, 6*, 1820-1837, 1994.

Jiménez, J., Intermittency and cascades, *Sci. Mar., 409*, 99-120, 2000.

Jou, D., Intermittent turbulence: a short introduction, *Sci. Mar., 61*, 57-62, 1997.

Kiørboe, T., Small-scale turbulence, marine snow formation, and planktivorous feeding, *Sci. Mar., 61*, 141-158. 1997.

Kitanidis, P.K., *Introduction to Geostatistics. Applications in Hydrogeology*. Cambridge University Press, 1997.

Kolmogorov, A.N., The local structure of turbulence in incompressible viscous fluid for very large Reynolds numbers. *Dokl. Akad. Nauk. SSSR , 30*, 299-303, 1941.

Legendre, L,. and P. Legendre, *Ecologie numérique*, Masson, 1984.

Lovejoy, S., W.J.S. Currie, Y. Teissier, M.E. Claereboudt, E. Bourget, J.C. Roff and D. Schertzer, Universal multifractals and ocean patchiness: phytoplankton, physical fields and coastal heterogeneity. *J. Plankton Res., 23*, 117-141, 2001.

Levine, E.R., and R.G. Lueck, Turbulence measurement from an autonomous underwater vehicle. *J. Atmos. Oceanic Technol., 16*, 1533-1544, 1999.

Lueck, R.G., and F. Wolk, An efficient method for determining the significance of covariance estimates. *J. Atmosp. Ocean. Tech., 16*, 773-775, 1999.

Lueck, R.G., D. Huang, D. Newman, and J. Box, Turbulence measurements with an autonomous moored instrument. *J. Atmos. Oceanic Technol., 14*, 143-161, 1997.

Muzy, J.F., J. Delour, and E. Bacry, Modelling fluctuations of financial time series: from cascade process to stochastic volatility model. *Eur. J. Phys. B, 17*, 537-548, 2000.

Obukhov, A.M., Spectral energy distribution in a turbulent flow. *Dokl. Akad. Nauk. SSSR, 32*, 22-24, 1941.

Obukhov, A.M., Structure of the temperature field in a turbulent flow. Izv. *Akad. Nauk. S.S.S.R.,Geogr. I Jeofiz., 13, 55*, 1949.

Osborn, T., Finestructure, microstructure, and thin layers, *Oceanography, 11*, 36-43, 1998.

Parzen, E. *Stochastic Processes*, Holden day, 1962.

Pascual, M., F.A. Ascioti, and H. Caswell, Intermittency in the plankton: a multifractal analysis of zooplankton biomass variability, *J. Plankton Res., 17*, 1209-1232, 1995.

Pumir, A., A numerical study of the mixing of a passive scalar in three dimension in the presence of a mean gradient. *Phys. Fluids, 6*, 2118-2132, 1994a.

Pumir, A., Small-scale properties of scalar and velocity differences in three dimensional turbulence. *Phys. Fluids, 6*, 3974-3984, 1994b.

Samorodnitsky, G., and M.S. Taqqu, *Stable Non-Gaussian Random Processes: Stochastic Models with Infinite Variance*, Chapman & Hall, New York, 1994.

Schertzer, D., and S. Lovejoy, Physical modeling and analysis of rain and clouds by anisotropic scaling multiplicative processes. *J. Geophys. Res., 92*, 96-99, 1987.

Schertzer, D., S. Lovejoy, and F. Schmitt, Structures in turbulence and multifractal universality. In *Small-scale Structure in 3D Fluid and MHD Tturbulence*, (M. Meneguzzi, A. Pouquet and P.L. Sulem, eds.), Springer-Verlag, New York, 137-144, 1995.

Schmitt, F., D. Lavallée, D. Shertzer, and S. Lovejoy, Empirical determination of universal multifractal exponents in turbulent velocity fields. *Phys. Rev. Lett., 68*, 305-308, 1992a.

Schmitt, F., D. Lavallée, S. Lovejoy, D. Schertzer, and C. , Hooge, Estimations directes des indices de multifractals universels dans le champ de vent et de température. *C. R. Acad. Sci. Paris Sér. II*, 314, 749-754, 1992b.

Schmitt, F., D. Schertzer, S. Lovejoy, and Y. Brunet, Estimation of universal multifractal indices for atmospheric turbulent velocity fields. *Fractals, 1*, 568-575, 1993.

Schmitt, F., D. Schertzer, S. Lovejoy, and Y. Brunet, Multifractal temperature and flux of temperature variance in fully developped turbulence. *Europhys Lett., 34*, 195-200, 1996.

Seuront, L., Space-time heterogeneity and biophysical couplins in pelagic ecosystems, PhD Thesis, Université des Sciences et Technologies de Lille, 1999.

Seuront, L., Microscale processes in the ocean: why are they so important for ecosystem functioning?, *La Mer, 39*, 1-8, 2001.

Seuront, L., and H. Yamazaki, Testing multiscaling statistics of ocean velocity fields in the inertial subrange, *in preparation*, 2001.

Seuront, L., F. Schmitt, D. Schertzer, Y. Lagadeuc, and S. Lovejoy, Multifractal intermittency of Eulerian and Lagrangian turbulence of ocean temperature and plankton fields, *Nonlin. Proc. Geophys., 3*, 236-246, 1996a.

Seuront, L., F. Schmitt, Y. Lagadeuc, D. Schertzer, S. Lovejoy, and S. Frontier, Multifractal analysis of phytoplankton biomass and temperature in the ocean, *Geophys. Res. Lett., 23*, 3591-3594, 1996b.

Seuront, L., F. Schmitt, Y. Lagadeuc, D. Schertzer, and S. Lovejoy, Universal multifractal analysis as a tool to characterize multiscale intermittent patterns: example of phytoplankton distribution in turbulent coastal waters, *J. Plankton Res., 21*, 877-922, 1999.

Seuront, L., V. Gentilhomme, and Y. Lagadeuc, Small-scale nutrient patches in tidally mixed coastal waters. *Mar. Ecol. Prog. Ser., accepted*, 2001a .

Seuront, L., F. Schmitt, and Y. Lagadeuc, Turbulence intermittency, small-scale phytoplankton patchiness and encounter rates in plankton: where do we go from here?, *Deep-Sea Res. I, 48*, 1199-1215, 2001b.

Seuront, L., F. Wolk, H. Yamazaki, and F. Schmitt, Universality of turbulent velocity and scalar fields fluctuations in the atmosphere and the ocean, *in preparation*, 2001c.

Seuront, L., H. Yamazaki, A. Nihongi, and F. Wolk, Bio-physical properties of a tidal channel. I. Observations of phytoplankton and turbidity fine-scale distributions, *in preparation*, 2001d.

Seuront, L., H. Yamazaki, J.G. Mitchell, and F. Schmitt, Biophysical properties of a tidal channel. II. Analysis of phytoplankton and turbidity microscale distributions *in preparation*, 2001e.

Sreenivasan, K.R., Fractals and multifractals in turbulence. *Ann. Rev. Fluid Mech., 23*, 539-600, 1991.

Takasugi, Y., A. Hoshika, H. Noguchi, and T. Tanimoto, The role of tidal vortices in material transport around straits. *J. Oceanogr., 50*, 65-80, 1994a.

Takasugi, Y., T. Fujiwara, and T. Sugimoto, Formation of sand banks due to tidal vortices around straits. *J. Oceanogr., 50*, 81-98, 1994b.

Tennekes, H., and J.L. Lumley, *A First Course in Turbulence*, MIT Press, Boston, 1972.

Visser, A.W., Using random walks models to simulate the vertical distribution of particles in a turbulent water column, *Mar. Ecol. Prog. Ser., 158*, 275-281, 1997.

Yamazaki, H., Lagrangian study of planktonic organisms: perspectives, *Bull. Mar. Sci., 53*, 265-278, 1993.

Yamazaki, H., T. Osborn, and K.D. Squires, Direct numerical simulation of planktonic contact in turbulent flow, *J. Plankton Res., 13*, 629-643, 1991.

Wolk, F., and R.G. Lueck, Heat flux and mixing efficiency in the surface mixing layer, *J. Geophys. Res., submitted*, 2001.

Wolk, F., L. Seuront, and H. Yamazaki, Spatial resolution of a new micro-optical probe for chlorophyll and turbidity. *J. Tokyo University. Fish., 87*, 13-21,2001.

Wolk, F., H. Yamazaki, L. Seuront, and R.G. Lueck, A new free-fall profiler for measuring biophysical microstructure. *J. Atmos. Oceanic Tech., accepted*, 2001.